JOURNAL OF GUIDANCE, CONTROL, AND DYNAMICS
Vol. 21, No. 3, May–June 1998

Ramjet-Powered Reusable Launch Vehicle Control by Sliding Modes

Christian Tournes,* D. Brian Landrum,† Yuri Shtessel,‡ and Clark W. Hawk§
University of Alabama in Huntsville, Huntsville, Alabama 35899

One possible approach to pitch control of an air-breathing reusable launch vehicle is differential throttling of opposite engines mounted on the conical lifting body. The vehicle must operate over a large range of flight regimes. The problem is aggravated by the relatively large angle of attack, which produces nonsymmetrical engine operation. The dynamics of controlling supersonic compression inlets also requires very rapid response times. A pitch controller architecture is proposed based on the sliding mode control (SMC) approach. SMC is a robust, nonlinear control technique characterized by its total insensitivity to matched disturbances and its perfect rejection of unmatched disturbances. The pitch control of a conical reusable launch vehicle by opposite engines operating in ramjet mode is simulated. In response to pitch-induced disturbances, the SMC controller accurately tracks the prescribed nominal moment through generation of required engine thrust profiles. The control occurs in a minimum settling time with no chatter.

Introduction

THE use of rocket-based combined cycle (RBCC) propulsion systems in reusable launch vehicles (RLVs) has received considerable attention in recent years. A 1992 workshop[1] recommended that a systems-level study be conducted to quantify the benefits and costs associated with RBCC systems and to define propulsion and vehicle technology requirements. Earlier studies had defined a baseline conical lifting body and specified the various engine configurations and their modes of operation according to the portion of the flight segment flown.[2] These studies also recommended installing the engines on the maximum diameter of the vehicle and using differential throttling as the preferred control mechanism. Engine control, specifically throttling and the control of air intake, was recognized as a primary technical challenge that needed to be addressed. An RBCC engine must operate over a wide range of operating conditions from launch to orbit. Without loss of generality, this article concentrates on an ejector scramjet operating in ramjet mode.

As shown in Fig. 1, the compression of the incoming airflow occurs in two steps. The first step is performed by the oblique forebody shock wave, which sets the inlet conditions for the second step. The second stage is assumed to be a supersonic compression inlet. The typical RLV flight profile requires a relatively large angle of attack. This produces reduced forebody compression on the upper surface and much stronger compression on the lower surface. The upper and lower engines must operate under very different input conditions satisfying the local flight condition, that is, the local pressure, Mach number, angle of attack, and oblique shock conditions.

Effective use of differential throttling of opposing engines as a pitch or yaw actuator requires the ability to create significant thrust variations with a relatively high characteristic frequency.[3] The controller must asymptotically track the thrust profile of each engine required to produce a desired pitching moment. The controller must also regulate the operation of the air intakes. Two control parameters are used: the cross-sectional area of the air intakes and the fuel/air mixture ratio. The moment created by differential throttling of the engines modifies the vehicle angle of attack and, hence, the asymmetrical shocks on the upper and lower sides of the forebody. Therefore, there is a strong coupling between the vehicle aerodynamics, engine performance, and vehicle control. The control of engine thrust and the regulation of the air intakes must be decoupled. The control problem posed is nonlinear and largely uncertain, with a large variation of operating conditions. The proposed controller must be insensitive to, or otherwise must be able to reject, any disturbances.

Previous researchers have proposed using μ controllers.[3] Sliding mode control (SMC) is an alternative nonlinear, robust control technique. When the uncertain terms are in the range space of the input matrix, this control approach is totally insensitive to matched disturbances and, otherwise, perfectly rejects unmatched disturbances. An estimation of the disturbances is not required, only the bounds of their uncertainty.[4–7] This makes the SMC technique ideal for solving a multiple input/multiple output (MIMO), nonlinear, and largely uncertain control problem. Application of the SMC technique for controlling high-performance aircraft has been demonstrated in previous studies.[7,8]

This paper discusses the use of differential throttling of opposing RLV engines to produce a desired pitching moment. A pitch control design methodology is proposed based on the SMC technique. First, the steady-state equations used to model the nominal flight performance of the upper and lower engines are presented. Next, simplified differential equations describing the dynamic response of the engines to changes in the control parameters are derived. The control model state differential equations are then presented, followed by the SMC controller design and architecture. Finally, the suitability of the SMC controller is demonstrated through simulation of the pitch control of a typical RLV by differential throttling of opposing ramjet engines.

Ramjet Engine Model

Forebody Compression

The proposed SMC solution is demonstrated through simulation of the pitch control of a typical ramjet-powered RLV shown schematically in Fig. 1. In the subsequent derivations the indices U and L are used to designate upper and lower surface flow variables, respectively. Also shown in Fig. 1, variable indices are likewise associated with the following engine flow path regions: ∞ in the freestream flow before the oblique shock, 1 aft of the oblique shock, 2 at the inlet section, m in the minimum area throat section, 3/4 before and after the internal shock, 5/6 at the beginning and end of combustion, and 7 in the nozzle exit section. A nominal cruising flight condition at a Mach number of 5, an altitude of 80 kft, and an angle of attack α of 6 deg is assumed.

Assuming a conical forebody half-angle of 8 deg, the upper surface will compressively turn the freestream flow by an angle of

Received May 7, 1997; revision received Oct. 20, 1997; accepted for publication Oct. 23, 1997.

*Ph.D. Student, Department of Electrical and Computer Engineering, EB 267. Senior Member AIAA.
†Assistant Professor, Propulsion Research Center, Department of Mechanical and Aerospace Engineering, RI E-33. Senior Member AIAA.
‡Associate Professor, Department of Electrical and Computer Engineering, EB 263-F.
§Professor and Director, Propulsion Research Center, RI E-26. Associate Fellow AIAA.

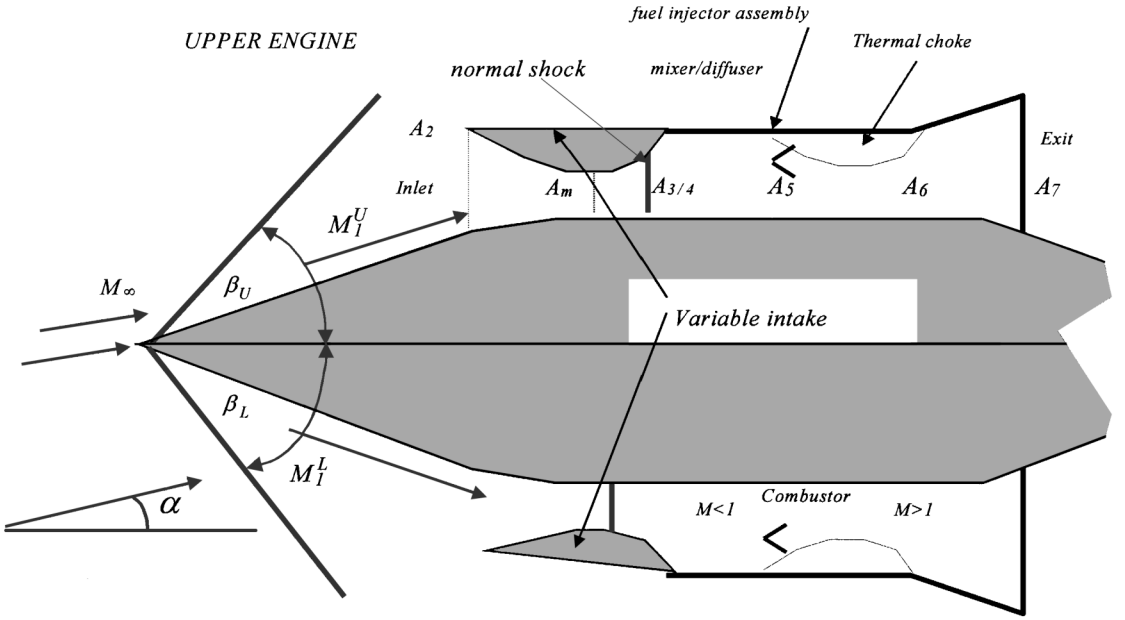

Fig. 1 Schematic of RLV forebody and propulsion system configuration.

2 deg, whereas the lower surface flow will be deflected 14 deg. The conical forebody shock is approximated by a two-dimensional oblique shock. Property changes across the oblique shock are determined by the normal component of the Mach number defined by $M_{n\infty} = M_\infty \sin\beta$, where β is the oblique shock wave angle.[9] Based on the assumed Mach number and altitude, the freestream static pressure and temperature are 2376 Pa and 220 K, respectively. The stagnation pressure and temperature are 1.5 MPa and 1326 K, respectively. The upper oblique shock wave angle is $\beta_U = 13$ deg. The Mach number behind the upper shock wave is $M_1^U = 4.76$, and the compression efficiency, i.e., the stagnation pressure ratio across the shock, is $\eta_{\infty/1}^U = P_1^U/P_\infty = 0.998$. For the lower oblique shock the corresponding values are $\beta_L = 24$ deg, $M_1^L = 3.6$, and $\eta_{\infty/1}^L = 0.74$.

Air Inlet Operation

As shown in Fig. 1, the ramjet has a variable inlet area A_2. The flow is compressed as the area converges from A_2 to the minimum area A_m at the throat section. The area then diverges with a normal shock occurring at section $A_{3/4}$. It is assumed that A_m can also be adjusted to maintain $M_m = M_3/1.2$. This prevents minor variations in the choking conditions driving the normal shock from the diverging to the converging side of the throat. The area of sections m and 3/4 are, thus, related to the inlet area A_2 by

$$A_m = A_2 \frac{\Sigma(M_3/1.2)}{\Sigma(M_2)}, \qquad A_3 = A_2 \frac{\Sigma(M_3)}{\Sigma(M_2)} \tag{1}$$

where

$$\Sigma(M) = (1/M)\cdot\{[2/(\gamma+1)]+[(\gamma-1)/(\gamma+1)]\cdot M^2\}^{(\gamma+1)/[2\cdot(\gamma-1)]} \tag{2}$$

Here, γ is the local ratio of specific heats.

In ramjet mode, the conditions in section 5 at the entrance to the combustor are given by

$$M_5 = \Sigma^{-1}(\Sigma_5), \qquad \Sigma_5 = A_5/A_2 \cdot \Sigma_2 \cdot \eta_{\text{frict}} \cdot \pi(M_3, \gamma_3) \tag{3}$$

and

$$P_5 = P_2 \cdot \eta_{\text{frict}} \cdot \pi(M_3, \gamma_3), \qquad T_5 = T_2 = T_\infty \tag{4}$$

where Σ^{-1} is the inverse function of Σ, η_{frict} is frictional pressure loss, and $\pi(M, \gamma)$ is the efficiency, i.e., the stagnation pressure ratio, of the upstream normal shock wave.[9] Fuel injection in section 5 increases the stagnation temperature, whereas the stagnation pressure decreases as a consequence of thermal choking. The steady-state combustion stagnation temperature T_6 required to achieve choking (that is, for $M_6 = 1$) is given by

$$T_6 = T_5\left[\frac{\phi(M_6)}{\phi(M_5)}\right]^2, \qquad \phi(M) = \frac{M\{1+[(\gamma-1)/2]\cdot M^2\}^{0.5}}{1+\gamma\cdot M^2} \tag{5}$$

The stagnation pressure loss resulting from thermal choking η_{ch} is given by

$$\eta_{\text{ch}} = \frac{\lambda(M_5)}{\lambda(M_6)}, \qquad \lambda(M) = \frac{1+\gamma M^2}{\{1+[(\gamma-1)/2]M^2\}^{\gamma/(\gamma-1)}} \tag{6}$$

The stagnation pressure ratio through the combustion section is a function of η_{ch} and the frictional pressure losses, or

$$P_6/P_5 = \eta_{\text{ch}}\eta_{\text{frict}} \tag{7}$$

Using the specific combustion energy of hydrogen gas,[10] the combustion efficiency η_{comb}, and an approximate relation for enthalpy, $H = [R\cdot\gamma/(\gamma-1)]T$, the relative hydrogen mass flow required to obtain the desired temperature T_6 is

$$\varepsilon = \frac{1.02\cdot[\gamma_6/(\gamma_6-1)]T_6 - [\gamma_5/(\gamma_5-1)]T_5}{491.7\cdot\eta_{\text{comb}}} \tag{8}$$

The total mass flow rate $\dot{m}_c$ is calculated from the air mass flow rate $\dot{m}_a$ by

$$\dot{m}_c = \dot{m}_a\cdot(1+\varepsilon) = \frac{k(\gamma,\varepsilon)\cdot P_6\cdot A_6^*}{T_6^{0.5}} \tag{9}$$

where

$$k(\gamma,\varepsilon) = \left[\frac{\gamma}{287.04\cdot(1-9\varepsilon)+462\cdot\varepsilon}\right]^{0.5} \times\left[\frac{\gamma+1}{2}\right]^{-(\gamma+1)/[2\cdot(\gamma-1)]} \tag{10}$$

In Eqs. (9) and (10) a constant combustion section area of $A_6 = A_6^* = A_5 = 1$ m^2 is assumed.

Nozzle

The need to operate over an extremely large range of flight conditions precludes the use of an adaptive nozzle, the dimensions of which would also be prohibitive. Using a control volume approach, the thrust F is calculated as the difference between the exit static

Table 1 General engine characteristics

Variable	Value	Variable	Value	Variable	Value
P_∞	1.5 MPa	T_∞	1324 K	$A_5 = A_6$	1 m^2
η_{nozzle}	0.95	η_{comb}	0.95	η_{fric}	0.95
P_5/P_4	0.95	ω_T	250 rad/s	A_7	7 m^2
η_{ch}	0.79	ω_5	55 rad/s	M_7	3.2

Table 2 Upper and lower engine nominal operating conditions

Variable	Upper	Lower	Variable	Upper	Lower
M_2	4.76	3.63	A_2	7.0 m^2	3.7 m^2
M_m	1.79	1.34	A_m	0.49 m^2	0.53 m^2
M_3	2.15	1.64	$A_{3/4}$	0.65 m^2	0.62 m^2
M_4	0.55	0.66	P_4/P_3	0.65	0.88
M_6	0.34	0.36	$\dot{m}_a$	453 kg/s	480 kg/s
T_6	3,000 K	2,800 K	ε	0.02	0.018
p_7	16,820 Pa	12,510 Pa	I_{sp}	2,950 s	3,150 s

pressure force and momentum and the input static pressure force and momentum:

$$F = \dot{m}_a \cdot [(1+\varepsilon)\cdot V_7 - V_\infty] + A_7 \cdot p_7 - A_\infty \cdot p_\infty \tag{11}$$

An arbitrary expansion area ratio of 62 is chosen, which yields a corresponding Mach number at the exit section 7 of $M_7 = 3.2$. The resultant specific impulse is calculated by

$$I_{\text{sp}} = \frac{F}{\dot{m}_a 9.81 \cdot \varepsilon} \tag{12}$$

Nominal Conditions

Table 1 lists general engine characteristics. Table 2 shows values for various upper and lower engine parameters under nominal operating conditions. These values were chosen to satisfy the following criteria: first, the need to have identical upper and lower engine thrusts with different inlet stagnation pressures and Mach numbers and, second, the need to achieve adequate values for specific impulse. A zero static margin was also assumed for convenience.

Engine Response Dynamics

The engine performance equations presented to this point are for steady-state operation and do not include derivatives of time. There are no closed-form solutions of unsteady aerothermodynamic problems, and applicable numerical methods are still largely in their infancy. Therefore, the dynamic response of the engines is approximated as follows.

Hydrogen Combustion

Combustion is unsteady and can be stable or unstable. The combustion temperature in section 6 is, therefore, modeled as a transfer function:

$$T_6 = \frac{(Q_{H_2}/Cp_6)\varepsilon + (Cp_5/Cp_6)\cdot T_5}{(s+\tau_{\text{comb}})\left[s^2 + 2\xi\cdot\omega_T s + (1-\xi^2)\omega_T^2\right]} \tag{13}$$

The real eigenvalue $\tau_{\text{comb}} = 2000$ rad/s represents the ignition and reaction time constant.[10] The imaginary conjugated eigenvalues are assumed to have a characteristic frequency of $\omega_T = 250$ rad/s. This value was chosen to represent one of the tangential acoustic modes, which is considered to be the most difficult to control, particularly in cylindrical chambers.[10] The unstable value of the exponential growth, $\xi = -0.1$, was chosen to illustrate the capability of the controller to control unstable plants.

Choking Dynamics

Thermal choking in section 6 produces a static pressure rise, which propagates as a sonic wave forward to section 4. The rise in the static pressure reduces the Mach number and, hence, the mass flow. The propagation velocity is the speed of sound, which depends on the local static temperature. The propagation also takes place within a variable Mach number flow $M(x)$. The calculation of the forward propagation time constant Δ_{46} can only be solved numerically. The numerical integration of the propagation time is decomposed into two segments based on the assumed temperature variation.

In the segment from section 6 to 5, the stagnation temperature $T(x)$ is assumed to vary exponentially according to

$$T(x) = T_6 - (T_6 - T_5)\cdot \exp\left(\frac{x - x_6}{x_6 - x_5}\right) \tag{14}$$

The variation of the local Mach number is determined from the thermal choking condition as

$$M(x) = \phi^{-1}\left\{\phi_6 \cdot [T(x)/T_6]^{0.5}\right\} \tag{15}$$

The corresponding propagation time constant within this segment is calculated using Eqs. (14) and (15) and the relation

$$\Delta_{65} = \int_{x_6}^{x_5} \frac{\mathrm{d}x}{[M(x)-1]\cdot\left[\gamma_7 \cdot R_{\text{air}+H_2O}\cdot T(x)\{1+[(\gamma-1)/2]M(x)^2\}^{-1}\right]^{0.5}} \tag{16}$$

In the segment from section 5 up to the normal shock wave at section 4 the stagnation temperature is constant, $T_4 = T_\infty$. The sectional area variation must be designed to provide a smooth and slow Mach number variation. This variation can be approximated in the calculation of the propagation time of the pressure wave by a linear variation of the local Mach number given by

$$M(x) = M_4 - (M_4 - M_5)\cdot\left(\frac{x - x_4}{x_5 - x_4}\right) \tag{17}$$

The resultant time constant associated with the forward movement of the choking condition within this segment is calculated using Eq. (17) and

$$\Delta_{54} = \int_{x_5}^{x_4} \frac{\mathrm{d}x}{[M(x)-1]\cdot\left(\gamma\cdot R_{\text{air}}\cdot T_4\cdot\{1+[(\gamma-1)/2]M(x)^2\}^{-1}\right)^{0.5}} \tag{18}$$

As the pressure wave generated by thermal choking propagates forward to section 4, the local Mach number and, hence, the position and efficiency of the normal shock wave are modified. The resultant response of Σ_5 to a change in T_6 is approximated by

$$\dot{\Sigma}_5 = -\frac{\Sigma_5}{\Delta_{65}+\Delta_{54}} + \frac{\Sigma\left\{\phi^{-1}\left[\phi_6\cdot(T_\infty/T_6)^{0.5}\right]\right\}}{\Delta_{65}+\Delta_{54}} \tag{19}$$

where $M_5 = \Sigma^{-1}(\Sigma_5)$.

Mechanical Area Variation

The areas of the inlet section 2 and of the throat section m are variable. This variation is assumed to be performed using hydraulic jacks. Similar to Ref. 3, their response functions are represented by

$$\begin{aligned}\ddot{A}_2 &= -1.4\omega_{A2}\dot{A}_2 + \omega_{A2}^2(-A_2 + A_{2-\text{com}})\\ \ddot{A}_m &= -1.4\omega_{A2}\dot{A}_m + \omega_{A2}^2(-A_m + A_{m-\text{com}})\end{aligned} \tag{20}$$

The assumed characteristic frequency of $\omega_{A2} = 50$ rad/s is comparable to current hydraulic jacks used in aviation. Although A_m is not a control variable per se, it must be adjusted in conjunction with A_2 to provide a sufficient safety margin guaranteeing sonic throat conditions.

Control Model

State Variables

The dynamics of the upper and lower engines are weakly coupled. The behavior of each engine is described by the following state variables: the value of the Mach function at the beginning of combustion $\Sigma_5(M_5, \gamma_5)$, the combustion stagnation temperature T_6, and the engine inlet area A_2. Equations (21–23) describe the engine state variables. State equation (21) describes the time derivative of T_6 and is derived from Eq. (13). The higher frequency real eigenvalue is two orders of magnitude larger than the characteristic frequency of the sliding surface and is stable. It is, therefore, acceptable to not include it in the design of the controller, although retaining it in the simulation. State equation (22) describing the time derivative of the Mach function Σ_5 is derived from Eq. (19). It uses the results of the numerical integration of Eqs. (14–18). State equation (23) governing the response of the engine inlet area is repeated from Eq. (20) for completeness,

$$\ddot{T}_6 = 50 \cdot \dot{T}_6 + \alpha \cdot (-T_6 + \beta \cdot (1 + d_\varepsilon) \cdot \varepsilon + \nu \cdot T_\infty) \tag{21}$$

$$\dot{\Sigma}_5 = -\omega_5 \Sigma_5 + \omega_5 \cdot \left(\Sigma \left\{ \phi^{-1} \left[0.4767 \cdot (T_\infty / T_6)^{0.5} \right] \right\} + d_\Sigma \right) \tag{22}$$

$$\ddot{A}_2 = -1.4\omega_{A2}\dot{A}_2 + \omega_{A2}(-A_2 + A_{2-\mathrm{com}} + d_A) \tag{23}$$

Controls and Outputs

The hydrogen/air mixture ratio ε and the prescribed inlet area $A_{2-\mathrm{com}}$ are used as controls. Normalized engine thrust f and normal shock wave efficiency $\eta_{3/4}$ are the system outputs. Equation (24) for the normalized thrust is derived from Eq. (11). The normal shock wave efficiency, calculated by Eq. (25), is obtained using conservation of mass between sections 2 and 5:

$$f = F/F_{\mathrm{nom}} = a \cdot A_2 \cdot (1 + \varepsilon) \cdot T_6^{0.5} + b \cdot A_2 + c \cdot A_2 \cdot \Sigma_2 \tag{24}$$

$$\eta_{\frac{3}{4}} = d \cdot A_2 \cdot \Sigma_5 (1 + d_\eta) \tag{25}$$

Although Eqs. (21–25) apply to both engines, their coefficients are different. The various coefficients used in these equations for the upper and lower engines are specified in Table 3.

Disturbances

The state equations (21–23) and output equation (25) also include disturbance terms. Equation (21) includes a disturbance affecting combustion effectiveness. As discussed in Ref. 10, the combustion effectiveness varies with the intensity of combustion. In the range of this study $d_\varepsilon \sim -0.1$. The variable d_Σ in Eq. (22) represents the uncertainties in the calculations of internal flow aerothermodynamics, in particular the uncertainty in the value of γ. In Eq. (23), the variable d_A is an area disturbance that represents imperfections in the variable inlet and throat. The variable d_η in Eq. (25) represents a disturbance in the internal shock efficiency. This could be caused by phenomena such as shock/boundary-layer interactions.

Table 3 Coefficients of the system equations

Variable	Upper engine	Lower engine
a	0.00836	0.0169
b	−0.364	−0.727
c	0.024	0.047
d	0.051	0.0136
α	61,875	61,875
β	87,670	88,080
ν	0.92	0.91

Problem Formulation

The control problem is broken into three segments: filtering of the prescribed moment command, thrust tracking, and shock regulation.

Moment Command

The flight control system generates a pitching moment command $M^*(t)$. The corresponding normalized thrust profile for each engine is given by

$$f^*_{L/U} = \frac{1 \pm M^*(t)/2 \cdot r_{\mathrm{ref}}}{s^3 + 1.75\varpi s^2 + 2.15\varpi^2 \cdot s + \varpi^3} \tag{26}$$

where r_{ref} represents the vehicle reference radius. Output tracking SMC requires the output and its derivatives included in the switching surface to be smooth. Therefore, the prescribed input generated by the flight control system must be smoothed. This is done by a third-order filter that minimizes the integral of the product of time and absolute error (an ITAE filter). The actuator's bandwidth is defined by choosing the characteristic frequency of the filter. As proposed by other researchers,[3] a value of $\varpi = 30$ rad/s was chosen. The control must also be able to augment or reduce the thrust of either engine by up to 20%.

Thrust Tracking

The control must asymptotically track the prescribed normalized values of the upper and lower engine thrusts. The behavior of the tracking error is defined by the switching surface design. The asymptotic tracking is given by

$$f_i^*(t) \forall i = \overline{U, L}, \qquad \lim_{t \to \infty} e_i = \lim_{t \to \infty} \left| f_i^* - f_i \right| = 0 \tag{27}$$

A switching surface characteristic frequency of 60 rad/s was chosen as double the characteristic frequency of the filter generating the signal to track.

Shock Regulation

The control must also track the prescribed efficiency of the shocks occurring in the internal compression inlets of the upper and lower engines. The asymptotic tracking relation is governed by

$$\eta^{*i}_{\frac{3}{4}}(t) \forall i = \overline{U, L}, \qquad \lim_{t \to \infty} e_i = \lim_{t \to \infty} \left| \eta^{*i}_{\frac{3}{4}} - \eta^{i}_{\frac{3}{4}} \right| = 0 \tag{28}$$

The prescribed values vary slowly according to the flight profile. The tracking error's behavior is defined by the switching surface. Its characteristic frequency is also 60 rad/s.

To provide a high-accuracy robust tracking of the prescribed moment, the following problems must be solved[7]:

1) For each flight condition, nominal thrust and the nominal efficiency of the internal shocks corresponding to an equilibrium condition must be calculated.

2) The command inputs must be filtered to smooth the prescribed thrust profiles and to introduce the desired response dynamics.

3) Controllers that track the prescribed thrust values and regulate the efficiencies of the internal shocks need to be designed. The controllers must provide the desired behavior of the thrust and shock efficiency tracking errors. They must also allow the system state to reach the switching surface in finite time and govern the motion of the system in this surface thereafter.

4) Because engine thrust is not measurable, a thrust estimator is required. There are two approaches for the design of such an estimator. The first approach is a nonlinear observer using measurements of, or deducing from measurements, the engine state variables. The second approach is based on estimating the pitching moment from inertial measurements of the pitch angle, the flight-path angle, and the pitch rate. The precision of this type of estimator is contingent on the accuracy of the aerodynamic model, current mass, and moments of inertia. The design of an engine thrust estimator is a challenging problem, which must be viewed in the context of solving the broader problem of pitch and yaw rate controller design. This broader problem will be addressed in future work.

In this study, thrust values used in the calculation of the switching surface are calculated by Eq. (24). This assumes an exact knowledge

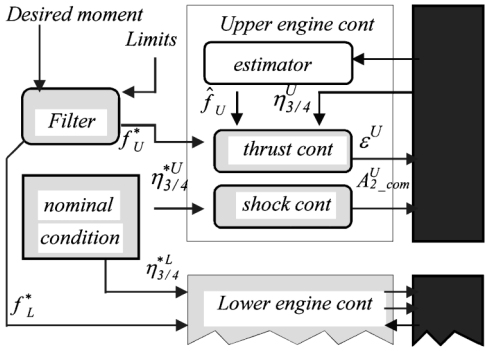

Fig. 2 Control architecture.

of the corresponding variables. The objective of this initial work is to show that it is possible to use differential engine throttling as a pitch and yaw actuator. The next step will be to show that differential throttling can be used to control pitch and yaw rates.

Control Architecture

The proposed control architecture is shown in Fig. 2. The desired steady-state pitching moment is M_{desired}. This moment must be created by the difference in the thrusts of the opposing engines. The filter generates the normalized prescribed thrust profiles f_U^* and f_L^* as represented by Eq. (26). The other command inputs are the desired values of the efficiencies of the normal shocks in the inlets $\eta_{3/4}^{*U}$ and $\eta_{3/4}^{*L}$. The prescribed efficiencies are necessarily different for the upper and lower engines.

For each engine, it is necessary to track the desired thrust and to regulate the efficiency of the internal shock. The thrust is controlled by the fuel mixture ratio ε and the inlet section area command $A_{2-\text{com}}$. The shock efficiency is regulated using only the inlet section area command.

SMC Design

Although the upper and lower engines are not totally decoupled, we assume here that they can be controlled separately. Their designs are, thus, identical, but with different operating parameters corresponding to different nominal conditions. The equations representing the upper or lower engine are

$$\dot{\boldsymbol{x}} = \boldsymbol{f}(\boldsymbol{x},t) + \Delta\boldsymbol{f}(\boldsymbol{x},t) + [\boldsymbol{B}(\boldsymbol{x},t) + \Delta\boldsymbol{B}(\boldsymbol{x},t)]\boldsymbol{u} \qquad \boldsymbol{y} = \boldsymbol{h}(\boldsymbol{x}) \quad (29)$$

The matrix $x = \{T_6, \Sigma_5, A_2\}^T$ includes the combustion stagnation temperature, the ratio of the area of section 6 to the corresponding critical area, and the inlet section area. The matrix $y = \{f, \eta_{3/4}\}^T$ includes the engine thrust and internal shock efficiency. The matrix $u = \{\varepsilon, A_{2-\text{com}}\}^T$ includes the fuel/air mixture ratio and the inlet section area command.

The systems considered are nonlinear MIMO systems, where $\boldsymbol{x} \in \boldsymbol{R}^3$ and $\boldsymbol{y} \in \boldsymbol{R}^2$. The functions $\boldsymbol{f}(\boldsymbol{x},t)$ and $\Delta\boldsymbol{f}(\boldsymbol{x},t)$ and the column matrices $\boldsymbol{B}(\boldsymbol{x},t)$ and $\Delta\boldsymbol{B}(\boldsymbol{x},t)$ are smooth vector fields. Here, $\Delta\boldsymbol{f}(\boldsymbol{x},t)$ and $\Delta\boldsymbol{B}(\boldsymbol{x},t)$ represent uncertain functions that arise from the uncertainty in the local value of γ. Such disturbances appear in the exponents of the functions $\Sigma(M,\gamma)$ and $\Sigma(M,\gamma)^{-1}$.

The various efficiency coefficient values used in this study are based on engineering approximations. Also, the models for combustion and the forward propagation of the choking conditions are based on relatively simplistic assumptions. Any imperfection in the tracking of the angle of attack will result in forebody shock conditions different from the nominal mode. The nominal system is obtained when $\Delta\boldsymbol{f}(\boldsymbol{x},t)$ and $\Delta\boldsymbol{B}(\boldsymbol{x},t) = 0$. Having defined reference trajectories f^* and $\eta_{3/4}^*$, the problem is to design a control function, $u(\varepsilon, A_{2-\text{com}})$, such that in the closed loop the output y tracks the prescribed output reference trajectories, or

$$\lim_{t\to\infty} e_i = \lim_{t\to\infty} \left[y_i^*(t) - y_i(t)\right] = 0 \quad (30)$$

The SMC controller design consists of the following three steps.[4–6]

1) Design the switching surface. The switching surfaces for thrust and shock efficiency are chosen such that the system's motion exhibits the desired output tracking errors:

$$\sigma_f = \left(\frac{\mathrm{d}}{\mathrm{d}t} + 1.4\omega_f + \omega_f^2 \int_0^t \mathrm{d}\tau\right)(f^* - f) = 0$$

$$\omega_f = 60\ \text{rad/s} \quad (31)$$

$$\sigma_\eta = \left(\frac{\mathrm{d}}{\mathrm{d}t} + 1.4\omega_\eta + \omega_\eta^2 \int_0^t \mathrm{d}\tau\right)\left(\eta_{\frac{3}{4}}^* - \eta_{\frac{3}{4}}\right) = 0$$

$$\omega_\eta = 60\ \text{rad/s} \quad (32)$$

Again, the characteristic frequency of 60 rad/s is chosen as twice the characteristic frequency of the filter generating the signal to track.

The system of Eq. (29) is transformed to a normal form with tracking variables f and $\eta_{3/4}$. Twice differentiating the two output vectors along the trajectory yields Eq. (33) for each engine. The terms $L^2 f$ and $L^2\eta_{3/4}$ represent the second trajectory derivatives with respect to the state variables. The design of the controller does not require their calculation, only the upper bound of their magnitudes. The second 2×2 matrix on the right-hand side of Eq. (33) represents the second trajectory derivatives relative to the state variables and to the controls. This matrix is nonsingular. The application of Lyapunov's linearization method to Eq. (22) shows that the internal dynamics variable Σ_5 in Eq. (34) is asymptotically stable to the equilibrium position:

$$\begin{bmatrix} \ddot{f} \\ \ddot{\eta}_{\frac{3}{4}} \end{bmatrix} = \begin{bmatrix} L^2 f \\ L^2 \eta_{\frac{3}{4}} \end{bmatrix} + \begin{bmatrix} 0.5aA_2\dfrac{1+\varepsilon}{T_c^{0.5}}\alpha\beta & a(1+\varepsilon)T_c^{0.5} + b + c\Sigma_5 \\ 0 & d\Sigma_5\omega_{A2}^2 \end{bmatrix} \cdot \begin{bmatrix} \varepsilon \\ A_{2-\text{com}} \end{bmatrix} \quad (33)$$

$$\dot{\Sigma}_5 = -\omega_5\Sigma_5 + \omega_5 \cdot \left(\Sigma\left\{\phi^{-1}\left[0.4767 \cdot (T_\infty/T_6)^{0.5}\right]\right\} + d_\Sigma\right) \quad (34)$$

2) Design the controller. The discontinuous control law is designed to allow the system state to reach the switching surface in finite time and govern the system's motion in this surface thereafter. The motion of the system on the switching surface is defined as a sliding mode. The conditions required to obtain these motions are referred to as the existence conditions of sliding mode or the attractivity conditions. A Lyapunov-based design approach is used to derive the control law. Defining $c_{i,r_i-1} = 1 \forall i = \overline{1,m}$, the desired motion of the system of Eqs. (33) and (34) in σ space is governed by

$$\sigma_i^T\dot{\sigma}_i = \sum_{j=1}^{r_i} \sigma_i c_i^{j-1}\left(y_i^{*[j]} - y_i^{[j]}\right) < 0 \quad (35)$$

Equation (35) can be rewritten in matrix notation as

$$\sigma_i^T\dot{\sigma}_i = \boldsymbol{\sigma}^T\{\boldsymbol{\Phi}(\boldsymbol{Y}^*) - \boldsymbol{L} - \boldsymbol{JU}\} < 0 \quad (36)$$

where

$$\boldsymbol{\Phi}(\boldsymbol{Y}^*) = \left[\sum_{j=1}^{2} c_f^{i-1} f^{*[j]}, \sum_{j=1}^{2} c_\eta^{i-1}\eta_{\frac{3}{4}}^{*[j]}\right]^T \quad (37)$$

and

$$\boldsymbol{L} = \left[\sum_{j=1}^{2} c_i^{j-1} L^j f, \sum_{j=1}^{2} c_i^{j-1} L^j \eta_{\frac{3}{4}}\right]^T \quad (38)$$

Different types of control laws may be used to achieve global asymptotic stability of the equilibrium point $\sigma = 0$ and a finite reaching time.[4–7] The control law chosen in this study is represented by

$$\boldsymbol{u} = \boldsymbol{u}_{\text{eq}} - \boldsymbol{\rho}\boldsymbol{J}^{-1}\mathbf{SIGN}\,\sigma, \qquad \rho_{i,i} > 0 \quad (39)$$

where $\boldsymbol{u}_{\text{eq}} = \boldsymbol{J}^{-1}[\boldsymbol{\Phi}(\boldsymbol{Y}^*) - \boldsymbol{L}]$ is an equivalent control providing $\dot{\boldsymbol{\sigma}} = 0$, and $\mathbf{SIGN}\,\sigma = \{\text{sign}\,\sigma_1, \ldots, \text{sign}\,\sigma_m\}^T$. Plant uncertainties

preclude the exact computation of an equivalent control and its replacement by an estimated value. The corresponding controllers are represented by Eqs. (40) and (41). Matrix $\boldsymbol{\rho}$ is a diagonal matrix. The values of $\rho_f = 40{,}000$ and $\rho_{\eta 3/4} = 400$ are introduced in the calculation of these equations to obtain finite and acceptable reaching times of the surface by the system. These values also account for the errors in the estimation of u_{eq}, whether such errors arise from model uncertainties or from disturbances. This means that $\rho_{i,i} > \|\hat{u}_{\text{eq}_{i,i}} - u_{\text{eq}_{i,i}}\|$. Here we use the nominal values of ε and A_2 and $\hat{\varepsilon}$ and $\hat{A}_2$ for estimated equivalent control:

$$\begin{bmatrix} \varepsilon^U \\ A^U_{2-\text{com}} \end{bmatrix} = \begin{bmatrix} 0.02 \\ 7 \end{bmatrix} - \begin{bmatrix} 0.0034 & -0.004 \\ 0 & 1.28 \end{bmatrix} \begin{bmatrix} \operatorname{sign}\sigma^U_f \\ \operatorname{sign}\sigma^U_\eta \end{bmatrix} \tag{40}$$

$$\begin{bmatrix} \varepsilon^L \\ A^L_{2-\text{com}} \end{bmatrix} = \begin{bmatrix} 0.018 \\ 3.4 \end{bmatrix} - \begin{bmatrix} 0.003 & -0.0035 \\ 0 & 0.47 \end{bmatrix} \begin{bmatrix} \operatorname{sign}\sigma^L_f \\ \operatorname{sign}\sigma^L_\eta \end{bmatrix} \tag{41}$$

3) Implement the controllers. The implementation of a high-frequency relay controller is not possible in mechanical applications such as the vehicle of this study.[7] Therefore, a boundary layer is introduced in the switching control[6] to avoid applying a discontinuous control. The switching element $\operatorname{sign}\sigma_i$ can be replaced by a saturation function $\operatorname{sat}(\sigma_i/\delta_i)$, where δ_i represents the ith switching element boundary-layer thickness. Such controller design reduces the control activity and provides a smoother operation. But the price paid for this is an eventual steady-state error while the controller operates linearly and a loss of robustness within the boundary layer. When the controller operates linearly, it is simply a state linear controller designed using nonlinear techniques. But, outside the boundary layer, it provides a finite reaching time and a relatively significant robustness that pure linear controllers do not provide. Introducing the integral term in Eqs. (31) and (32) eliminates the steady-state output tracking errors. The final controller design is given by

$$\begin{aligned} \varepsilon^U &= 0.02 + 0.0135\operatorname{sat}\left(\sigma^U_f\right) - 0.016\operatorname{sat}\left(\sigma^U_\eta\right) \\ \varepsilon^L &= 0.018 + 0.012\operatorname{sat}\left(\sigma^L_f\right) + 0.015\operatorname{sat}\left(\sigma^L_\eta\right) \end{aligned} \tag{42}$$

and

$$A^U_{2-\text{com}} = 7 + 5.12\operatorname{sat}\left(\sigma^U_\eta\right), \qquad A^L_{2-\text{com}} = 3.7 + 1.88\operatorname{sat}\left(\sigma^L_\eta\right) \tag{43}$$

The amplitudes of the saturation functions are designed to take into account the amplitude of the control authority available.

It should also be noted that the $\hat{u}_{\text{eq}}$ values in Eqs. (42) and (43) are estimated by the nominal values of ε and of A_2. Such estimations by constant terms are very crude, and as a consequence, the amplitudes of the ρ_i values in Eq. (39) need to be relatively large.

Remark: The robustness of the control law given by Eqs. (42) and (43) arises from the selection of the control amplitudes on the basis of inequalities. The only quantitative knowledge of the plant required is the magnitude range of the components of the uncertain vectors $\Delta \boldsymbol{f}(\boldsymbol{x}, t)$ and $\Delta \boldsymbol{B}(\boldsymbol{x}, t)$.

Simulation Results

The pitching moment is normalized by the nominal thrust. In the following simulation, the maximum normalized amplitude of the prescribed moment equals 0.2. This value corresponds to a 10% engine thrust reduction or augmentation. The shock efficiencies of both engines are simply regulated at their nominal values. The simulation models the pitch control response of the vehicle in the presence of four imposed disturbances. Figure 3 shows the normalized pitching moment and the total net thrust. Figure 4 shows the tracking of the prescribed upper and lower engine thrusts. Figure 5 shows the error between the desired and actual moment. Figure 6 is a plot of the variation of stagnation combustion temperature and the corresponding fuel/air mixture ratio relative to stoichiometric conditions. Finally, Figs. 7 and 8 show the internal shock efficiencies and the variation of the inlet section area, respectively.

The response of the system to the four imposed disturbances is as follows:

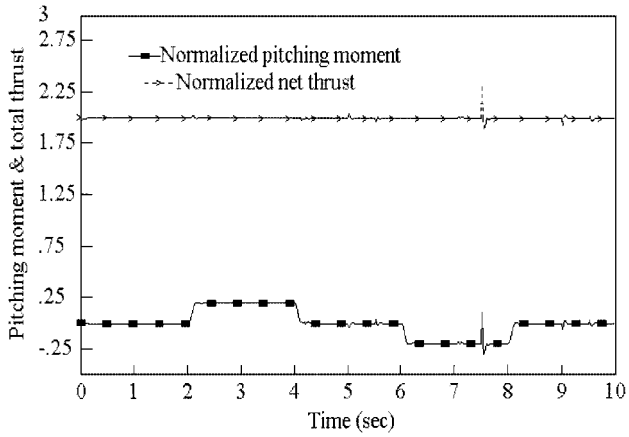

Fig. 3 Normalized pitching moment and total net thrust.

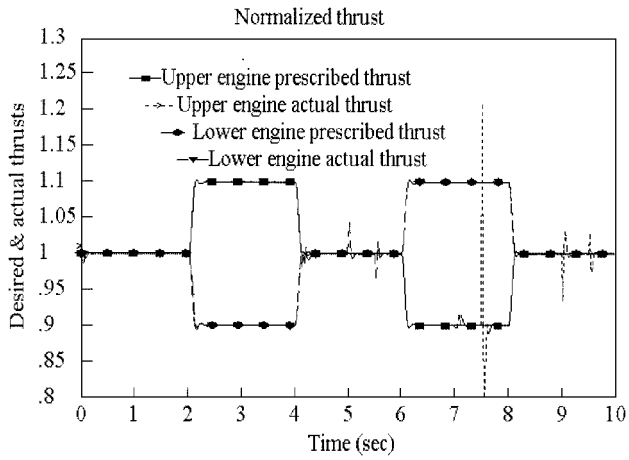

Fig. 4 Tracking of the prescribed upper and lower engine thrusts.

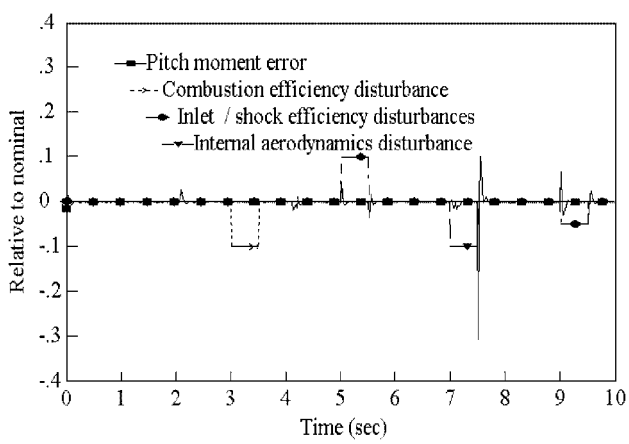

Fig. 5 Error between desired and actual pitching moment and effects of imposed disturbances.

1) The first disturbance reduces the combustion efficiency of the upper engine by 10% from $t = 3$ to 3.5 s. This is in the range space of the input matrix and is, thus, a matched disturbance. Figure 4 shows that the effects on the thrust are negligible. Figure 6 shows that temperature is not affected, but the fuel/air mixture ratio is increased by 10%.

2) The second disturbance increases the effective area of section 2 of the lower engine by 10% from $t = 5$ to 5.5 s. This is also a matched disturbance. However, unlike the preceding case, it affects both outputs as shown by Eqs. (23–25). Therefore, this disturbance also behaves as an unmatched disturbance. As shown in Fig. 7, the disturbance causes a small transient error in the regulation of the shock efficiency. The peak amplitude of this transient error is 0.016 and its settling time is 0.15 s. Figure 8 shows that the disturbance causes a small, essentially negligible transient modification of the

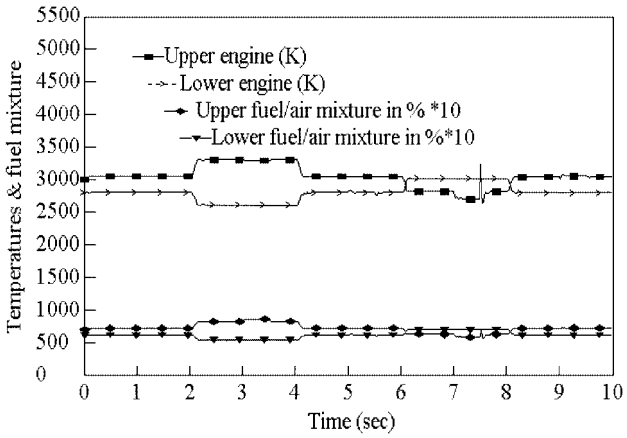

Fig. 6 Variation in combustion temperature and fuel/air mixture ratio relative to stoichiometric conditions.

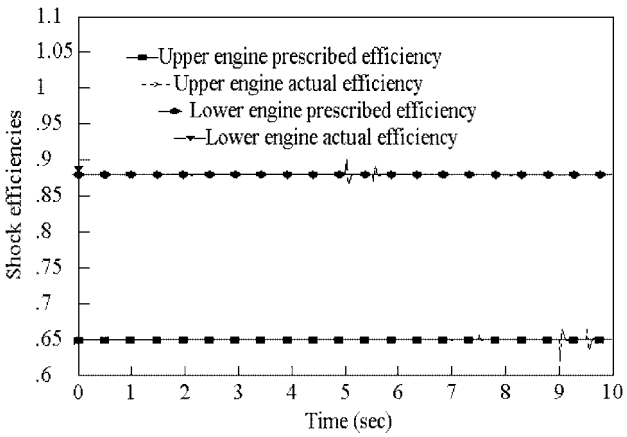

Fig. 7 Internal engine shock efficiencies.

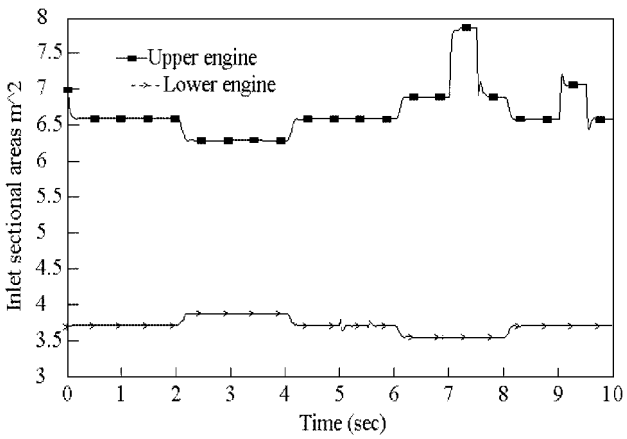

Fig. 8 Variation in inlet section area A_2 for the upper and lower engines.

inlet cross-sectional area. As seen in Figs. 4 and 5, the disturbance also induces a transient error on the tracking of prescribed thrust with a peak amplitude of 0.035 and a settling time of 0.15 s. The duration of the transient corresponds to the characteristic frequency of the sliding surfaces defined by Eqs. (31) and (32).

3) A third disturbance in the internal aerodynamics of the upper engine decreases the value of Σ_5 by 0.1 from $t = 7$ to 7.5 s. This unmatched disturbance directly affects the internal engine dynamics represented by Eq. (22). As a consequence, the fuel/air mixture ratio (Fig. 6) and inlet cross-sectional area (Fig. 8) of the upper engine are modified. As shown in Fig. 5, this causes a transient thrust tracking error with peak amplitude of 0.25 and a settling time of 0.25 s. A transient error in the regulation of shock efficiency (Fig. 7) is also induced with peak amplitude of 0.014 and a settling time of 0.005 s.

4) A fourth disturbance in the shock efficiency of the upper engine is introduced from $t = 9$ to 9.5 s. As shown in Fig. 7, the regulation of the shock efficiency rejects this disturbance. Its effect on the tracking of the prescribed thrust is shown in Fig. 4. The amplitude of the peak error is 0.023 with a settling time of 0.15 s. Although not shown, the differential throttling also modifies the engine specific impulses by 5%.

As seen in Fig. 5, the imposed disturbances do not introduce steady-state tracking errors. The error between the desired moment and the actual moment is relatively small. The results presented indicate that the tracking is accurate with a settling time of approximately 0.2 s. The response of all variables is smooth, and the controls do not chatter.

Conclusions

This paper addresses the control of the pitching moment of a reusable launch vehicle through differential throttling of opposing engines. The MIMO nonlinear control design is based on the SMC technique. The control architecture developed comprises a generation of the desired thrust profiles of the upper and lower engines. The thrust profiles are tracked by locally decoupled sliding mode controllers. The efficiencies of the normal shocks in the supersonic compression inlets of both engines are regulated to specific values corresponding to the nominal flight condition and in particular to the nominal angle of attack.

It is assumed that the vehicle is powered by RBCC engines operating in ramjet mode. An analytical model of the nominal flight performance of the engines and their dynamic response to changes in the control parameters is derived. Although simplistic, this model provides enough realism to support a first evaluation of the control architecture. Detailed numerical simulations of combustion dynamics could be conducted to provide a more refined model.

The suitability of the SMC controller is demonstrated through simulation of the pitch control response of the vehicle in the presence of four imposed disturbances. The matched and unmatched disturbances do not introduce steady-state tracking errors. The error between the desired moment and the actual moment is relatively small. The tracking is accurate with a minimal settling time. The response of all variables is smooth, and the controls do not chatter.

The feasibility of this differential throttling control should be further evaluated within the context of a full flight mechanics model. The capabilities should also be evaluated for other flight conditions and operating modes.

References

[1]Chojnacki, K. T., and Hawk, C. W., "Rocket Based Combined Cycle (RBCC) Propulsion Technology Workshop Proceedings Executive Summary," Propulsion Research Center, Univ. of Alabama, Huntsville, AL, Aug. 1992, pp. 5–7.

[2]Foster, R. W., Escher, W. J., and Robinson, J., "Air Augmented Rocket Propulsion Concepts," U.S. Air Force Astronautics Lab., AFAL-TR-88-004, Edwards AFB, CA, Jan. 1988.

[3]Buscheck, H., and Calise, A., "Hypersonic Flight Control System Design Using Fixed Order Robust Controllers," AIAA Paper 95-6062, April 1995.

[4]Utkin, V. I., "Systems with Scalar Control," *Sliding Modes in Control Optimization*, Springer-Verlag, Berlin, Germany, 1992, pp. 111–130.

[5]Fernandez, B. R., and Hedrick, K. J., "Control of Multivariable Non-Linear Systems by the Sliding Mode Method," *International Journal of Control*, Vol. 46, No. 3, 1987, pp. 1019–1040.

[6]Slotine, J., and Weiping, Li, "Direct Implementations of Switching Control Laws," *Applied Nonlinear Control*, Prentice-Hall, Englewood Cliffs, NJ, 1991, pp. 276–310.

[7]Tournes, C., and Shtessel, Y. B., "Aircraft Control Using Sliding Mode Control," AIAA Paper 96-3692, June 1996.

[8]Singh, S. N., Steinberg, M., and DiGirolamo, R. D., "Variable Structure Robust Flight Control Systems for the F-14," *IEEE Transactions on Aerospace and Electronics Systems*, Vol. 33, No. 1, 1997, pp. 77–84.

[9]Anderson, J. D., *Modern Compressible Flow*, McGraw–Hill, New York, 1990, pp. 100–120.

[10]Lieberherr, J. F., "Instabilites de Combustion (Combustion Instabilities)," Energetique Generale de Combustion Flammes et Foyers (*Energy Course Notes of Ecole Nationale Superieure de L'Aeronautique*), Ecole Nationale de l'Aeronautique, Toulouse, France, 1969, pp. 121–136 (in French).